A Raptor-based Adaptive Erasure Code over Ka-band Space Channel

Zhou Jie, Jiao Jian, Yang Zhi-hua, Gu Shu-shi, Zhang Qin-yu
Communication Engineering Research Center of HITSZ
Harbin Institute of Technology Shenzhen Graduate School
Shen Zhen, China
zqy@hit.edu

***Abstract*—In order to efficiently resist the influence of weather dynamics over Ka-band link, this paper designs a practical Raptor based erasure code combined with a forecast model, which has adaptive code rate on different weather. The forecast model could capture the weather correlation through the Gilbert-Elliot model, and lower the forecast errors by employing CFDP (CCSDS File Delivery Protocol) asynchronous NAKs (Negative Acknowledgement) to feed back the channel state information (CSI). We provide analytical results on forecast error and simulation shows that the algorithm can significantly enhance the decoding performance, especially in the bad weather state, and maintain the link availability and high throughput over Ka-band weather dependent link.**

Keywords-Ka-band; Raptor code; forecast model; CFDP asynchronous NAK mode

I. INTRODUCTION

The success of Mars Reconnaissance Orbiter (MRO) demonstrated the feasibility that future exploration missions employ the Ka-band [1-2]. Though 32GHz Ka-band signal increases the downlink throughput, file delivery is highly vulnerable to fluctuating weather states of ground station area and experiences severe errors which lead to frequent link outages [3-5]. For high reliable data return (i.e. with 99% weather availability), there is unexpectedly a 4.7 dB penalty at Ka-band compared to a 1.17 dB penalty at X-band [6].

To improve Ka-band link efficiency, many research focus on the rate adaption and long erasure correcting codes (LEC) at present [7-11]. The rate adaptive transmission scheme mitigates the adverse effect of fluctuation weather by dynamically adjusting the link margins, and it is also indicated the adaptive rate transmission scheme has significant advantages in the throughput and link availability compared to the constant rate transmission in [7], but there's no specific coding scheme and the Markov model used is less accurate. On the other hand, the existing LEC schemes are RS, LDPC (IRA code, GeIRA code) and LDGM codes. RS code has limited optional parameters and large complexity, and the LDPC code needs a long code-length. These limitations are beyond the capacity of the probers in processing and storage. Contrast to LDPC code, the rateless fountain code, as one of the LDGM codes, is more suitable to resist the burst error. Therefore, the paper discusses an adaptive concatenated erasure coding technique with small code-length and linear encoding and decoding complexity, which could mitigate the error-floor by concatenating a pre-coding scheme.

From the adaptive erasure code perspective, it is more meaningful to predict the weather state for the rate adaption. As a general method, Markov model could be exploited to forecast the weather state. However, the high forecast error in this model cannot meet the requirement of the reliable scientific data return. Hence, we propose a forecast model to degrade the forecast error, by employing CFDP asynchronous NAKs to feed back the channel state information (CSI). Based on the forecast model, we design a specific Raptor based erasure code with rate adaption to maintain link availability and high throughput. Raptor code, as a type of fountain code, could recover the whole file as the destination receives N packets a little more than k raw packets. Consequently the adaptive Raptor code could accommodate itself to the Ka-band weather dependent space channel.

The rest of this paper is organized as follows: Section II describes a Ka-band channel forecast model and gives the analytical results on the forecast error. The details of Raptor based concatenated erasure coding scheme are presented in Section III. Section IV discusses parameter design and throughput analysis of adaptive erasure coding scheme. In Section V, simulation and discussion are presented. Finally, Section VI gives the conclusion.

II. KA-BAND CHANNEL FORECAST MODEL

A. Gilbert-Elliot channel

Ka-band is highly vulnerable to weather impairments. The downlink data integrity is affected by packet errors badly, which are incurred by the system noise from the rain and cloudy. Therefore, it is necessary to establish a dynamics channel model to capture the weather correlation.

A rain attenuation of Ka-band model is built to simulate link burst BERs associated with the changing weather states in [3-5]. In this model, a noise temperature threshold is defined as T_{th}. If the sampled noise temperature is less than T_{th}, define the weather as good state, denoting it as G, and most of the transmitted packets will be received successfully; the space downlink is available with low BERs (10^{-8}~10^{-5}). Otherwise, it is defined as bad state, representing it as B, significant error

 ISBN: 978-1-61208-194-6

will occur for the high noise temperature of the receiver antenna. Relatively high BERs (10^{-4}~10^{-3}) are applied to capture severe packet loss rates (50%~99%), and make the link unusable. The dynamics of the Ka-band link are modeled as the Gilbert-Elliot model based on the AWGN channel, as shown in Fig. 1,

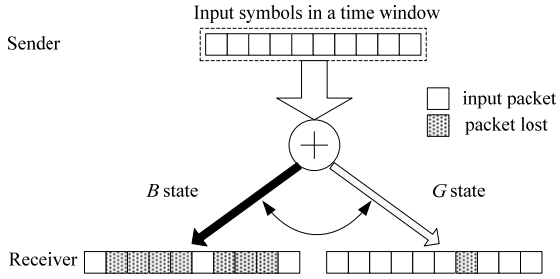

Figure 1. Two error state AWGN channel Gilbert-Elliot model

Suppose we use BPSK modulation and we have

$$BER = Q\left(\sqrt{2E_b/N_0}\right) \tag{1}$$

E_b/N_0 is the SNR, where $N_0 = K \cdot T_{th}$. Then, the relationship between noise temperature T_{th} and BER is:

$$T_{th} = \frac{2E_b}{K \cdot \left(Q^{-1}\left(BER\right)\right)^2} \tag{2}$$

In GE model, the next state is only determined by the current state, so we define the transfer probabilities from *G* to *B* as $P(B|G)= \lambda_G$, and from *B* to *G* state as $P(G|B)= \lambda_B$, respectively. The state transfer matrix $\boldsymbol{P}$ can be written as:

$$\boldsymbol{P} = \begin{bmatrix} P(G|G) & P(B|G) \\ P(G|B) & P(B|B) \end{bmatrix} = \begin{bmatrix} 1-\lambda_G & \lambda_G \\ \lambda_B & 1-\lambda_B \end{bmatrix} \tag{3}$$

Using standard methods, the eigenvalues of $\boldsymbol{P}$ are found to be $\lambda_1 = 1$ and $\lambda_2 = 1-\lambda_G-\lambda_B$, with corresponding eigenvectors $\boldsymbol{S_1} = \begin{bmatrix} 1 & 1 \end{bmatrix}^T$ and $\boldsymbol{S_2} = \begin{bmatrix} \lambda_G & -\lambda_B \end{bmatrix}^T$, where *T* denotes transpose. Consequently, we can write

$$\boldsymbol{P = S \Lambda S^{-1}} \tag{4}$$

where $\boldsymbol{S} = \begin{bmatrix} 1 & \lambda_G \\ 1 & -\lambda_B \end{bmatrix}$, $\boldsymbol{\Lambda} = \begin{bmatrix} \lambda_1 & 0 \\ 0 & \lambda_2 \end{bmatrix}$.

So the stationary probability of each state is:

$$\begin{aligned} P_G &= \lambda_B / \left(\lambda_G + \lambda_B\right) \\ P_B &= \lambda_G / \left(\lambda_G + \lambda_B\right) \end{aligned} \tag{5}$$

We define the matrix in (3) as the one-step transfer matrix, which can predict the next time weather state with the current state. And we define the matrix in (6) as the *m*-step transfer matrix, which can predict the weather state at the m^{th} instants of time with the current state.

$$\boldsymbol{P^m} = \boldsymbol{S \Lambda^m S^{-1}} = \begin{bmatrix} P_G \cdot \left(1-\lambda_2{}^m\right) + \lambda_2{}^m & P_B \cdot \left(1-\lambda_2{}^m\right) \\ P_G \cdot \left(1-\lambda_2{}^m\right) & P_B \cdot \left(1-\lambda_2{}^m\right) + \lambda_2{}^m \end{bmatrix} \tag{6}$$

Based on the Markov chain, if the channel at time 0 is in the *G* state, then the weather state forecast error at time *m* is $2 \times \left(P_G \cdot \left(1-\lambda_2{}^m\right) + \lambda_2{}^m\right) \cdot P_B \cdot \left(1-\lambda_2{}^m\right)$, while be in *B* state, then the forecast error is $2 \times P_G \cdot \left(1-\lambda_2{}^m\right) \cdot \left(P_B \cdot \left(1-\lambda_2{}^m\right) + \lambda_2{}^m\right)$. So the weather state forecast error $F_e(m)$ at time *m* associated with (5) is defined as:

$$\begin{aligned} F_e(m) = {} & P_G \cdot \left(2 \times \left(P_G \cdot \left(1-\lambda_2{}^m\right) + \lambda_2{}^m\right) \cdot P_B \cdot \left(1-\lambda_2{}^m\right)\right) \\ & + P_B \cdot \left(2 \times P_G \cdot \left(1-\lambda_2{}^m\right) \cdot \left(P_B \cdot \left(1-\lambda_2{}^m\right) + \lambda_2{}^m\right)\right) \end{aligned} \tag{7}$$

From (7), we can easily see the forecast error will become higher when the value of *m* increases. So we need exploit a high quality forecast model to reduce the error for the data integrity.

B. The forecast model based on the CFDP asynchronous NAK mode

CFDP provides a store-and-forward file delivery capability operating across an end-to-end space link [12-13]. In the acknowledged transmission mode, communication reliability is guaranteed through negative acknowledgment (NAK) issued by the CFDP receiving entity. Four NAK algorithms can be chosen to adopt the different scenarios. Considering the asynchronous NAK mode, the receiver can set a timer to control the file checking time and then feedback the results to ensure reliability [14]. In this paper, we build a weather state forecast model combined the asynchronous NAK mode, as shown in Fig. 2.

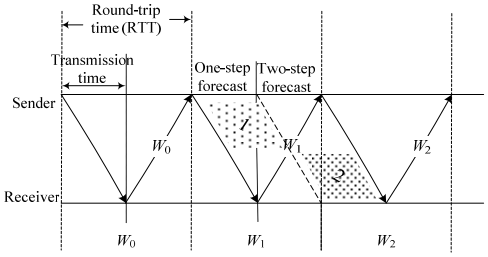

Figure 2. The weather state forecast model

In this forecast model, assume the duration of a weather state *W* is equal to round-trip time (RTT) and the duration of each transmission is the full resolution of the raw data, which is about 1.44 minute time scale, chosen to be consistent with [3].

We define the duration of each transmission as a time window. Upon receipt of the first packet, the receiver will feed back the CSI on current weather state every other RTT until the file ends. It is in the state W_1 that the sender will obtain the state W_0 feed backed by the receiver after experiencing a

 ISBN: 978-1-61208-194-6

transmission time. In this period W_1, it needs to predict two steps weather parameters according to the previous state W_0 through the forecast model, as shown in following steps:

a) one-step forecast area: the first part of data will reach the receiver being in this period W_1 after a downlink transmission time (as "1" in Fig. 2), we can get the rate parameter for coding these data, using one-step transfer matrix.

b) two-step forecast area: the second part will be sent during the second half of the state and then arrive the receiver at the next state W_2 (as "2" in Fig. 2), which can be predicted by two-step transfer matrix for the parameter.

As the one-step and two-step areas are the same length in the state W_1, the forecast error F_e is expressed by

$$F_e = 0.5 \times F_e(1) + 0.5 \times F_e(2) \quad (8)$$

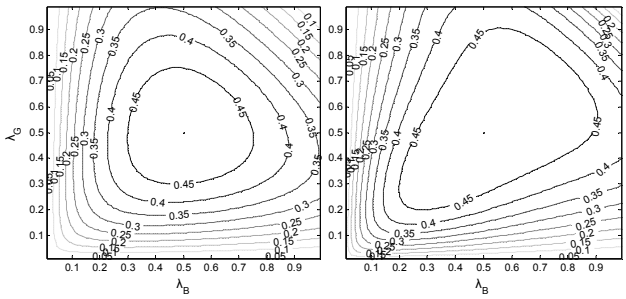

(a) One-step forecast error (b) Two-step forecast error

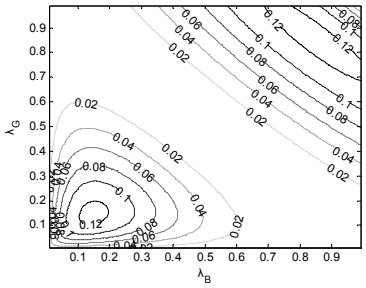

(c) The difference between the one-step and two-step forecast errors

Figure 3. Forecast error on different transition probabilities

The Fig. 3 shows the influence of different λ_B and λ_G on the one-step and two-step forecast errors. It can be seen that the error is close to maximum of 0.5 with both of the transfer probabilities tending to 0.5 gradually. If any probability is less than 0.05 or both exceed 0.95, the forecast error is within 10%. This result illustrates when one weather state is stable for a long time or two states switch steadily, the model has high forecast accuracy.

Compared with (a) and (b) in Fig. 3, the two-step forecast error tends to maximum rapidly, which means two-step forecast error is larger than the one-step forecast error, using the same transfer matrix. Moreover the forecast error is larger when the transfer probability deviate more from 0.5. On the other hand, the error falls back to 0, when both of the transfer probabilities are close to edge (0 or 1), as shown in Fig. 3(c). Compared to the Markov model in Fig. 1, the forecast model combined with the CFDP asynchronous NAK mode in Fig. 2 has a lower forecast error.

III. Design and Performance of Raptor-based Concatenated Erasure Coding Scheme

A. The design of concatenated erasure coding scheme

Based on the proposed forecast model, we design a concatenated erasure coding scheme with small code length and linear encoding and decoding complexity, as shown in Fig. 4.

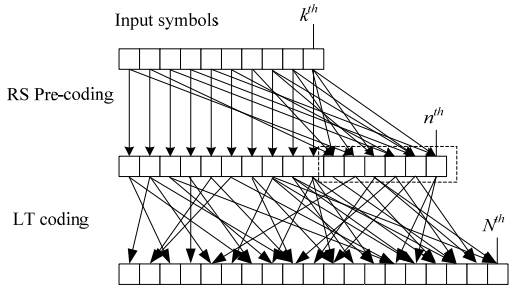

Figure 4. Raptor based concatenated erasure code scheme

The Raptor based concatenated erasure code parameter is defined as $(k, n, N, \mathbf{\Omega})$, where k is the original information packets, n is the intermediate packets, N is fountain code erasure packets and $\mathbf{\Omega}$ is degree distribution. The encoding process as follows:

a) genetate n intermediate packets from the k raw packets using RS pre-code.

b) generate N erausre packets from n intermediate packets using LT code with corresponding degree distribution.

And the decoding process as follows:

a) recovers n' $(\le n)$ intermediate packets from the received erasure packets using BP algorithm.

b) then recover corresponding raw packets from the n' intermidiate packets using RS decoding algorithm.

The BER determines the efficient values of k and n. The sender computes the BER related with a weather state to acquire code rate.

B. The encoding and decoding performance of concatenated erasure code

As mentioned above, RS code, as the pre-code of Raptor code, could recover the k raw packets from the n' intermediate packets LT code recovers. In this section, we use weaken robust soliton distribution (WRSD) as the degree distribution with linear complexity, which can recover the majority of raw packets [10]. The generator function is defined as:

$$\mathbf{\Omega}(x) = \left[ux + \sum_{i=2}^{D} x^i / \left(i \cdot (i-1)\right) + x^{D+1}/D \right] \Big/ (u+1) \quad (9)$$

If Raptor code adopts the WRSD, it has been proved that any set $(1+\varepsilon/2)\cdot n+1$ of received packets are sufficient to recover at least $(1-\delta)\cdot n, \left(\delta = (\varepsilon/4)/(1+\varepsilon)\right)$ intermediate packets via BP decoding, where the complexity is $O(\ln(1/\varepsilon))$.

 ISBN: 978-1-61208-194-6

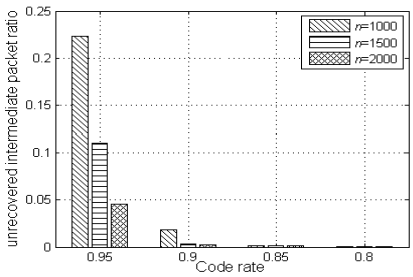

Figure 5. Recovery capability of fountain code with WRSD

Fig. 5 shows the relationship between code rate and unrecovered intermediate packet ratio as the raw packets are 1000, 1500 and 2000, respectively. It can be seen that the ratios are lower than 0.05 when code rate is less than 0.9. So we can recover all raw packets by means of adding the RS code with rate less than 0.95.

IV. Parameter Design and Throughput Analysis of Adaptive Erasure Coding Scheme

A. Parameter design of adaptive erausre code

As mentioned in Section II, the BER varies with weather states transition, and we accommodate the BER variations by designing an adaptive parameter coding scheme. For the BER value, the forecast model in Fig. 2 can obtain it by forecasting the weather state when data arrive at the receiver. Consequently, we can achieve rate adaption as follows.

Given a time window T, we assume the downlink data rate R and the code length L, then $N = T \cdot R / L$ erasure packets will be transmitted during a time window. The relationship between packet loss rate and BER becomes:

$$P_{packet} = 1 - (1 - BER)^{L} \tag{10}$$

The scheme handles the changing packet loss rates by adjusting code rates of the rateless fountain code adaptively.

GPC and BPC are defined as the G and B states parameter coding scheme respectively. We can receive N_G erasure packets successfully and recover k_G raw packets in G state with the BER P_{egood} and the same as N_B, k_B and P_{ebad} in B state. So the code rates of G and B state are given by:

$$Coderate_{good} = k_G / N \tag{11}$$

$$Coderate_{bad} = k_B / N \tag{12}$$

The above analysis in Fig. 5 explains that if the error correction capacity of RS code is more than δn, $(1 - P_{packet}) \cdot N$ erasure packets that the receiver get in certain BER, are sufficient to recover the entire file. When T and other communication conditions are fixed, the value of N is constant and there exist $P_{egood} \le P_{ebad}$ and $Coderate_{good} \ge Coderate_{bad}$. Hence, this paper proposes an adaptive parameter coding scheme APC, which accommodates the code rates of Raptor code adaptively based on the weather state transition. Its statistical average code rate during a time window is obtained as follows:

$$Coderate_{adaptive} = \frac{P_G \cdot k_G + P_B \cdot k_B}{N} \tag{13}$$

B. Analysis of link throughput

The GPC can recover the entire file in G state, but recover little in B state. A time window throughput of the GPC is represented by:

$$Throughput_{good} = P_G \cdot k_G \tag{14}$$

The BPC could recover all information in both states and then maintain the link availability. Its throughput in one time window is given by:

$$Throughput_{bad} = k_B \tag{15}$$

Compared with (14) and (15), the link occur outage when the GPC is in B state. On the other hand, though the BPC keeps the link continuous, it results in a small throughput. In this section, the proposed APC could maintain the link availability and high throughput by updating the parameters according to the CSI. Its statistical average throughput during a time window can be expressed by:

$$Throughput_{adaptive} = (P_G - F_e/2) \cdot k_G + P_B \cdot k_B \tag{16}$$

V. Simulation and Disscussion

We choose 20K as the noise temperature threshold in [3] and the one-step transfer matrix is defined as:

$$\boldsymbol{P} = \begin{bmatrix} 0.9773 & 0.0227 \\ 0.1667 & 0.8333 \end{bmatrix} \tag{17}$$

TABLE I. Simulation Parameters

Parameter	Value
Code length L	1Kbyte
A time window T	1.44min
Downlink data rate R	20KBps
Weather state probabilities	P_G=0.88, P_B=0.12
Erasure packets of each transmission N	1728
The weather state forecast error F_e	0.0869
BER	G state: 10^{-8}, 10^{-7}, 10^{-6}, 10^{-5} B state: 10^{-4}, 1.5×10^{-4}
GPC, BPC and APC code rates	G state: 0.828,0.824, 0.820,0.752 B state: 0.3357, 0.1325
LT code rates	G state: 0.69,0.689,0.684,0.614 B state: 0.2519, 0.1621

Table I shows the simulation parameters of GPC, BPC, APC and adaptive LT code for comparison. The values refer to the typical Earth-Mars communication scenario. Code rates are obtained by the corresponding simulation of coding schemes with the Monte Carlo under the decoding failure rate 10^{-4}. We execute 10000 simulations at each BER and average the result.

 ISBN: 978-1-61208-194-6

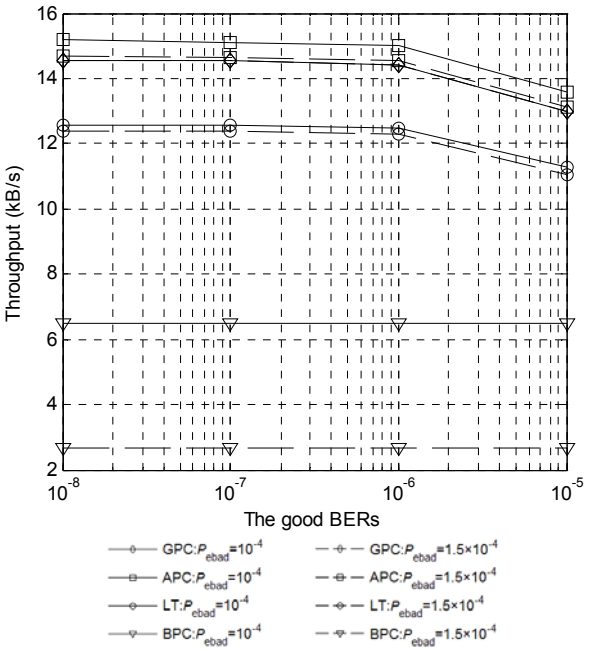

Figure 6. Throughput of GPC, BPC and APC with bad BER 10^{-4} and 1.5×10^{-4}. The throughput of the LT code is also included for comparison.

Fig. 6 shows the throughput in one time window of the GPC, BPC, APC and also adaptive LT code. It is indicated that with increased bad BER, the APC and LT coding schemes reduce their throughputs slightly, which illustrates that the bad BER is a factor of adaptive code throughput decline except the forecast error. Moreover, the proposed APC is superior to the adaptive LT code of same type with respect to throughput apparently. However, the throughput of GPC does not vary with the bad BERs since the link using GPC is equivalent to outage in the bad state. Similarly, the throughput of BPC is stable with the good BERs for $P_{egood} \le P_{ebad}$. Both the APC and GPC have significantly better throughput than the BPC has. The APC is close to the GPC on throughput, but keeps the link continuous compared to the GPC.

VI. Conclusion and Future Work

In this paper, for combating the adverse effects of frustration weather on data delivery, we design a Raptor based adaptive erasure coding scheme over a weather state forecast model, which has excellent encoding and decoding performance and low complexity. In the proposed scheme, CFDP asynchronous NAKs are employed to degrade the weather state forecast error. We design an adaptive parameter coding scheme APC on code rate, which could recover the total data especially in the bad weather state, enhance dramatically the decoding performance and keep the link available compared to the fixed parameter GPC. It also achieves 200% throughput increase compared to the reliable BPC and maintains high throughput. Therefore the adaptive erasure code is suitable for high-level reliable file delivery in exploration missions.

Systematic fountain code will be designed in the future work, in order to improve flexibility of encoding and decoding schemes.

Acknowledgment

This project has been supported by the Key Program of Natural Science Foundation of China (NSFC) under Grant No. 61032003 and Natural Science Foundation for the Youth (NSFY) under Grant No. 61102083.

References

[1] S. Shambayati, F. Bavarian, and D. Morabito. Link design and planning for Mars Reconnaissance Orbiter (MRO) Ka-band (32 GHz) telecom demonstration [C]. IEEE Aerospace Conference, May 2005, pp. 1559-1569.

[2] S. Shambayati. Deep space Ka-band link: design, continuity and completeness [C]. IEEE Aerospace Conference, March 2008, pp. 1-14.

[3] I. Sung and J. Gao. CFDP performance over weather-dependent Ka-band channel [C]. SpaceOps 2006 Conference, Rome, Italy, June 2006, pp. 1-21.

[4] B. Maruddan, A. Kurniawan, S. Sugihartono, and A. Munir. Performance evaluation of Ka-Band satellite communication system in rain fading channel at tropical area [C]. International Conference on Electrical Engineering and Informatics, July 2011, pp. 1-5.

[5] M. Felice, C. Candilio, H. Xiong, Q. Gao, and R. Ricardo. Long-term rain attenuation prediction for Ka-Band link over Venezuela [C]. 2010 5th International Conference on Pervasive Computing and Applications (ICPCA), 2010, pp. 46-49.

[6] G. Noreen, T. Komarek, and R. Diehl. Mars Telecommunications Orbiter Ka-band system design and operations [C]. 9th Ka-band Utilization Conference, Lacco Ameno, Italy, November 2003.

[7] J.Sun, J. Gao, and S. Shambayati. Ka-band link optimization with rate adaptation [C]. IEEE Aerospace Conference, March 2006, pp. 1-7.

[8] T. Cola, H. Ernst, and M. Marchese. Application of long erasure codes and ARQ schemes for achieving high data transfer performance over long delay networks [J]. Satellite Communications and Navigation, May 2008, pp. 643-656

[9] M. Luby. LT codes [C]. 43rd Annual IEEE Symposium on Foundations of Computer Science. Vancouver, BC, Canada, November 16-19, 2002.

[10] A. Shokrollahi. Raptor codes [J]. IEEE Transactions on Information Theory, vol. 52, no. 6, June 2006, pp. 2551-2567.

[11] Q. Li, L. Yin, and J. Lu. Application of LDPC codes for Deep Space Communication under Solar Scintillation Condition. ICOSSSE'11 Proceedings of the 10th WSEAS international conference on System science and simulation in engineering, 2011.

[12] J. Jiao, Q. Guo, and Q. Zhang. Packets Interleaving CCSDS File Delivery Protocol in Deep Space Communication [J]. IEEE Aerospace Electronic System Magazine, vol.26, no.2, 2011, pp. 5-11.

[13] F. Flentge. Study on CFDP and DTN Architectures for ESA Space Missions [C]. The Third International Conference on Advances in Satellite and Space Communications, 2011, pp. 75-80.

[14] J. Jiao, Q. Zhang, and H. Li. An Optimal ARQ Timer Design of file delivery time in CFDP NAK Model [C]. Wicom09, Beijing, 2009, pp. 3946-3950.

 ISBN: 978-1-61208-194-6